Remote Sensing of Environment 226 (2019) 16–25

Contents lists available at ScienceDirect

Remote Sensing of Environment

journal homepage: www.elsevier.com/locate/rse

Sampling depth of L-band radiometer measurements of soil moisture and freeze-thaw dynamics on the Tibetan Plateau

Donghai Zheng[a,*], Xin Li[a], Xin Wang[b], Zuoliang Wang[b], Jun Wen[c,**], Rogier van der Velde[d], Mike Schwank[e], Zhongbo Su[d]

[a] Institute of Tibetan Plateau Research, Chinese Academy of Sciences, Beijing, China
[b] Northwest Institute of Eco-Environment and Resources, Chinese Academy of Sciences, Lanzhou, China
[c] College of Atmospheric Sciences, Chengdu University of Information Technology, Chengdu, China
[d] Faculty of Geo-Information Science and Earth Observation, University of Twente, Enschede, the Netherlands
[e] Swiss Federal Research Institute WSL, Birmensdorf, Switzerland

ARTICLE INFO

Keywords:
L-band radiometry
Sampling depth
Diurnal variations
Grassland
Soil Moisture Active Passive (SMAP)
Soil Moisture and Ocean Salinity (SMOS)

ABSTRACT

Knowing the exact sampling depth of microwave radiometry is essential for quantifying the performance and appreciation of the applicability of satellite soil moisture products. We investigate in this study the sampling depth (δ_{SM}) of the L-band microwave emission under frozen and thawed soil conditions on the Tibetan Plateau. Two years of diurnal brightness temperature (T_B^P) measurements at a time interval of 30 min are collected by the ELBARA-III radiometer deployed at a Tibetan meadow site. Vertical profiles of soil temperature and volumetric liquid water content (θ_{liq}) are measured simultaneously at soil depths up to 1 m below the surface. The impact of the θ_{liq} measured at different depths on the microwave emission simulations is assessed using the τ-ω emission model, whereby the permittivity of frozen and thawed soil is estimated by the four-phase dielectric mixing model. It is found that: 1) the sampling depth for the effective temperature depends on the magnitude of θ_{liq}, and is estimated to be, on average, about 50 and 15 cm for the cold dry and wet warm period, respectively, because of the seasonality in θ_{liq}; 2) the δ_{SM} is determined at 2.5 cm for both frozen and thawed soil conditions during both cold and warm periods, which is shallower than the commonly used θ_{liq} measurement depth (i.e. 5 cm) adopted for the in-situ monitoring networks across the globe; 3) the T_B^P simulations performed with the θ_{liq} measurements taken at the estimated δ_{SM} of 2.5 cm result in lower unbiased root mean squared errors, about 14% (3.16 K) and 22% (3.36 K) for the horizontal and vertical polarizations respectively, in comparison to the simulations with the θ_{liq} measurements taken from 5 cm soil depth; and 4) the θ_{liq} retrieved with the single channel algorithm from the ELBARA-III measured vertically polarized T_B^P are in better agreement with the θ_{liq} measured at 2.5 cm than the one measured at 5 cm. These findings are crucial for developing strategies for the calibration/validation as well as the application of satellite based soil moisture products relying on the L-band radiometry.

1. Introduction

Surface soil moisture and freeze-thaw dynamics are key state variables controlling water and heat exchanges at the land-atmospheric interface and regulating the hydrologic cycle (Koster et al., 2004; Jin et al., 2009; Li et al., 2012; Zheng et al., 2018a). L-band (1.4 GHz, 21 cm) radiometry is recognized as one of the best suitable techniques for global monitoring of soil moisture and freeze-thaw dynamics (Entekhabi et al., 2010; Kerr et al., 2012; Wigneron et al., 2017). Two currently operational satellite missions make use of this technology, namely, Soil Moisture Active Passive (SMAP) launched by National Aeronautic and Space Administration (NASA) in 2015 (Entekhabi et al., 2010), as well as Soil Moisture and Ocean Salinity (SMOS) launched by European Space Agency (ESA) in 2009 (Kerr et al., 2001). Over the past decade, numerous studies were conducted to evaluate and improve the retrievals of surface soil moisture and freeze/thaw state obtained by these two missions (Rautiainen et al., 2014; Rautiainen et al., 2016; Derksen et al., 2017; Chan et al., 2018).

Several field campaigns were developed for assessment of the satellite based brightness temperature (T_B^P) and soil moisture products

* Correspondence to: D. Zheng, Institute of Tibetan Plateau Research, Chinese Academy of Sciences, 100101 Beijing, China.
** Correspondence to: J. Wen, College of Atmospheric Sciences, Chengdu University of Information Technology, 610225 Chengdu, China.
E-mail addresses: zhengd@itpcas.ac.cn (D. Zheng), jwen@cuit.edu.cn (J. Wen).

https://doi.org/10.1016/j.rse.2019.03.029
Received 28 November 2018; Received in revised form 14 February 2019; Accepted 22 March 2019

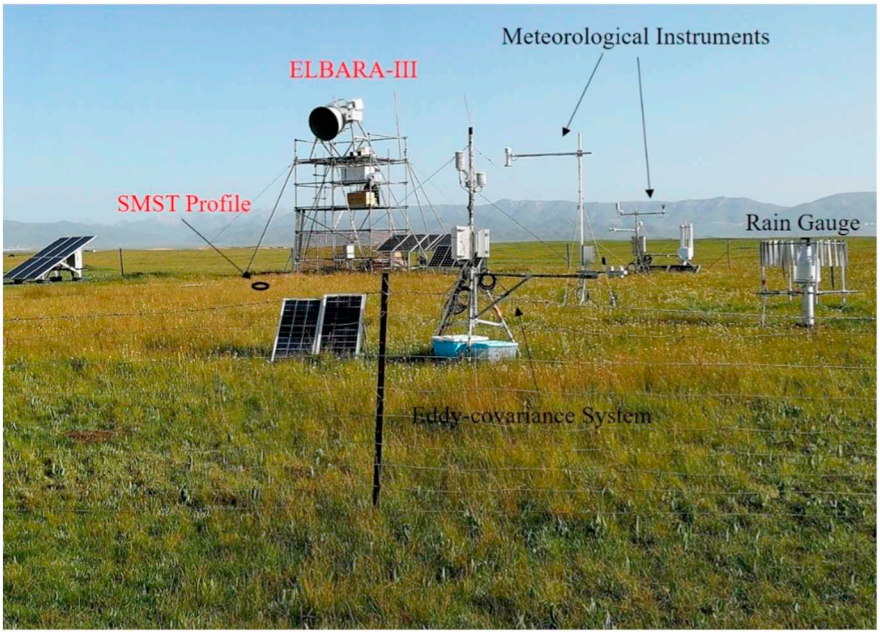

Fig. 1. Overview of ELBARA-III field site and deployed measurements.

using L-band microwave measurements collected from ground and aircraft-based platforms. For instance, SMOS validation campaigns were carried out in Valencia (Spain) (Schwank et al., 2012), Rur and Erft catchment (Germany) (Montzka et al., 2013), Sodankylä (Finland) (Rautiainen et al., 2012) and Grenoble (France) (Pellarin et al., 2016) across diverse land covers and climatic regions. Also a series of field experiments were designed in support of the SMAP mission, such as SMAPEx (Panciera et al., 2013), SMAPVEX12 (Mcnairn et al., 2015) and SMAPVEX15 (Colliander et al., 2017a). Besides, a set of soil moisture validation sites deployed over various land cover types under different climatological conditions was mobilized by the SMAP mission (Colliander et al., 2017b) to quantify the worldwide performance of soil moisture retrievals. Part of these efforts have focused on the Tibetan Plateau, where various in-situ soil moisture monitoring networks are operated (Su et al., 2011; Yang et al., 2013; Chen et al., 2017). Since January 2016, one of the ESA funded ELBARA-III radiometers (Schwank et al., 2010) is deployed in one of these in-situ networks (Zheng et al., 2017). Biases were reported for soil moisture products produced by the SMAP and SMOS missions based on comparisons with the measurements collected by the in-situ soil moisture monitoring networks maintained on the Tibetan Plateau (Dente et al., 2012; Chen et al., 2017; Li et al., 2018; Zheng et al., 2018b). Systematic dry biases were noted for both SMAP and SMOS products across different land covers and climate zones on the plateau, which was attributed to the presence of Radio Frequency Interference (Dente et al., 2012), or the use of imperfect parameterizations for the soil effective temperature (Chen et al., 2017) and surface roughness (Zheng et al., 2018b).

However, the soil moisture measurements utilized for the above assessments are usually taken at a soil depth of 5 cm that does not necessarily match the sampling depth of microwave emission at L-band, which thus brings uncertainty in the evaluation results. The soil moisture sampling depth (δ_{SM}) is generally determined as the depth of the soil layer whose dielectric properties dominate the emissivity of surface soil (Wang, 1987; Escorihuela et al., 2010). The δ_{SM} is directly a function of the wavelength (λ) of microwave emission, and both experimental and theoretical investigations indicated that the δ_{SM} is about one-tenth of a λ, i.e., 2.1 cm for the L-band radiometry measurements (Wilheit, 1978; Wang, 1987; Raju et al., 1995; Escorihuela et al., 2010). The δ_{SM} also depends on the soil moisture conditions as reported by Escorihuela et al. (2010) among others. Moreover, Zheng et al. (2017), Roy et al. (2017), Rowlandson et al. (2018) and Williamson et al. (2018) recently reported that the T_B^P signatures of ground-based L-band radiometry measurements are also highly sensitive to the diurnal freeze-thaw dynamics of surface soil layer (~2.5 cm). The changing permittivity of the surface soil layer caused by the freeze–thaw transition dominates the diurnal cycle of T_B^P measurements (Zheng et al., 2017). Both theoretical research and experimental research suggest that the sampling depth of the L-band radiometry is shallower than 5 cm at which the soil moisture measurements are commonly taken. The impact of surface soil moisture measurement depths (i.e. 5 cm vs. 2.5 cm) on the land surface emission simulations under both frozen and thawed soil conditions needs to be further investigated.

We investigate in this study the sampling depth of L-band radiometry under frozen and thawed soil conditions at a site on the Tibetan Plateau. Correlation analysis is performed between the ELBARA-III measured T_B^P and in-situ measurements of liquid water content (θ_{liq}) taken at different soil depths, and the τ-ω emission model is adopted for assessing the impact of surface θ_{liq} taken from different depths on the microwave emission simulations. The ELBARA-III radiometer (Schwank et al., 2010) is deployed in a Tibetan meadow ecosystem to measure the T_B^P at L-band every 30 min since January 2016, and a vertically dense measurement profile of soil moisture and soil temperature (SMST) sensors is installed at the following depths: 2.5, 5, 7.5, 10, 12.5, 15, 17.5, 20, 25, 30, 35, 40, 45, 50, 60, 70, 80, 90, and 100 cm (Zheng et al., 2017; Lv et al., 2018).

This paper is organized as follows. In Section 2 we present the ELBARA-III measured T_B^P and in-situ SMST measurements, the adopted land surface emission model and the soil moisture retrieval algorithm. The correlation analysis between T_B^P measurements and soil moisture sampling depths δ_{SM} is presented in Section 3, whereby the impact of δ_{SM} on the L-band land surface emission simulations is also discussed. Section 3 also provides the comparison between θ_{liq} retrievals from the ELBARA-III measurements and in-situ surface θ_{liq} taken from different depths. The findings are summarized in Section 4.

2. Materials and methods

2.1. ELBARA-III field site and measurements

The ELBARA-III radiometer is deployed in a Tibetan meadow

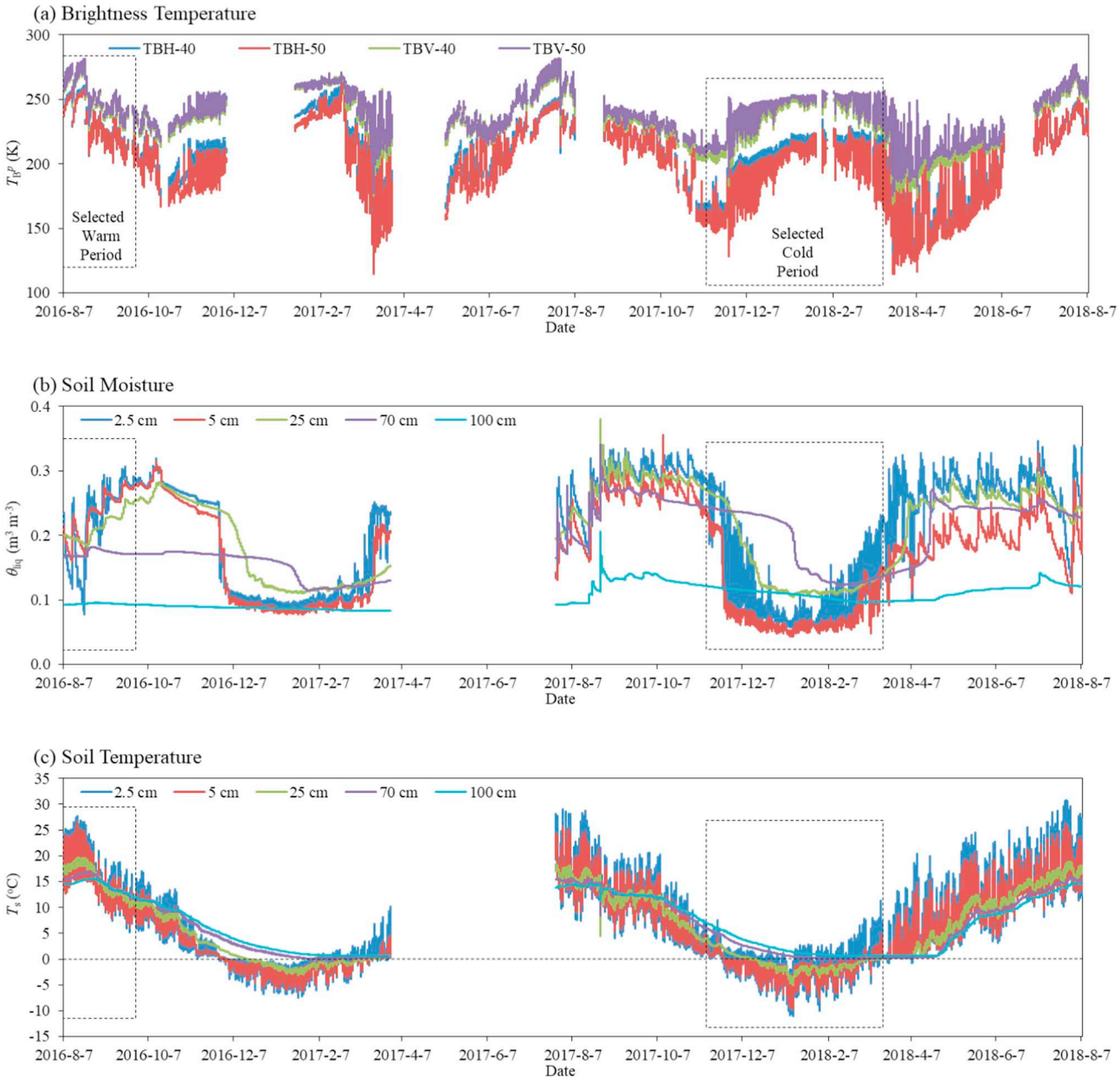

Fig. 2. Time series of measured (a) T_B^H and T_B^V at incidence angles of 40° and 50°, (b) θ_{liq} and (c) T_s at soil depths of 2.5, 5, 25, 70 and 100 cm with a time interval of 30 min from 7 August 2016 to 7 August 2018. Two selected cold and warm periods are also shown.

ecosystem situated in the northeastern part of the Tibetan Plateau, where a well-instrumented in-situ SMST monitoring network was developed (Zheng et al., 2017). The soil type of ELBARA-III field site is sandy loam with on average 2.2% clay, 49.7% sand, and a bulk density of $\rho_b \cong 1$ g cm^{-3} for the surface soil layer. The radiometer is mounted on a tower with a height of 4.8 m in the beginning of 2016, and the antenna beam waist is about 6.5 m above the surface (Fig. 1). The T_B^p measurements with vertical (T_B^V) and horizontal (T_B^H) polarizations are performed every 30 min at observation angles of 40° to 70° in steps of 5°. A sky measurement with an observation angle of 155° is performed once per day for calibration purposes next to the internal calibration sequence performed as part of every measurement run. Raw data of each ELBARA-III measurement are voltage samples consisting of 2400 measurements performed at the sampling rate of 800 Hz across an integration time of 3 s (Schwank et al., 2010; Naderpour et al., 2017). The internal calibration adopted to derive the T_B^p from the raw data is based on a two-point calibration strategy using a resistive load (RL) and an active cold load (ACL). The RL is kept at the accurately stabilized instrument internal temperature with an accuracy better than 0.1 K, and the ACL is calibrated by means of cold sky measurements. A detailed description of the ELBARA-III T_B^p measurements and data processing is outlined in Zheng et al. (2017), and readers are referred to Schwank et al. (2010) and Naderpour et al. (2017) for additional information on the ELBARA-III instrument and the calibration protocol for its measurements.

Concurrent measurements of micrometeorological variables are performed in vicinity of the radiometer tower (Fig. 1), such as solar radiation, wind speed, air temperature, air pressure, and humidity. A rain gauge and eddy-covariance system are setup in the ELBARA-III field site at the end of 2016 providing precipitation and surface heat flux measurements. Besides, a vertically dense SMST measurement profile is installed in August 2018, which is equipped with decagon 5TM capacitance probes and EM50 data loggers that records the measurements every 15 min. The SMST at each depth is measured with a single 5TM probe.

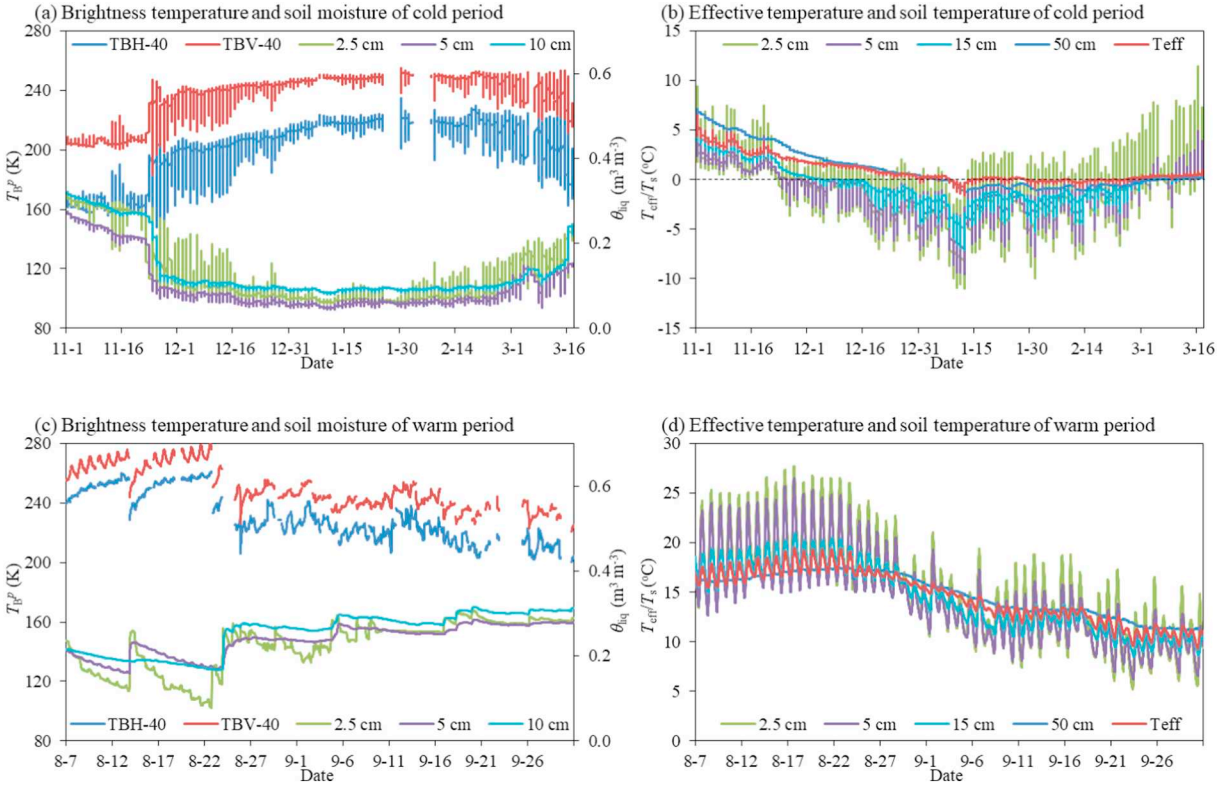

Fig. 3. Time series of (a, c) measured T_B^p at incidence angle of 40° and θ_{liq} at soil depths of 2.5, 5 and 10 cm, and (b, d) measured T_s at soil depths of 2.5, 5, 15 and 50 cm as well as estimated T_{eff} with a time interval of 30 min for the selected cold (2017.11.1–2018.3.17) and warm (2016.8.7–2016.9.30) periods.

2.2. Land surface emission model and soil moisture retrieval algorithm

The zero-order τ-ω microwave emission model (Mo et al., 1982) is widely adopted for the forward land surface emission modelling, e.g. by both SMAP (O'Neill et al., 2015; Chan et al., 2018) and SMOS (Kerr et al., 2012; Wigneron et al., 2017) missions. Recently, Schwank et al. (2018) showed that the performance of τ-ω model in simulating the T_B^p is comparable to that of the multiple-scattering two-stream microwave emission model for weakly scattering vegetation. Zheng et al. (2018c) also found that the performance of τ-ω model can be enhanced by implementing the values of vegetation opacity and effective scattering albedo derived from the two-stream model for the Tibetan grasslands. New vegetation and surface roughness parameterizations were proposed in Zheng et al. (2018c) to mitigate the overestimation of vegetation effect and underestimation of surface roughness effect that were found for the default SMAP parameterizations for the Tibetan environment. In addition, the permittivity (ε_s) of frozen and thawed soil was estimated using the four-phase dielectric mixing model (Schwank et al., 2004). In this study, the modified microwave emission model described in Zheng et al. (2018c) is adopted for estimating the L-band land surface emission, whereby the effective temperature (T_{eff}) is estimated as (Choudhury et al., 1982):

$$T_{eff} = \int_0^\infty T_s(z)\alpha(z)\exp\left[-\int_0^z \alpha(z')dz'\right]dz \quad (1)$$

$$\alpha(z) = \frac{4\pi}{\lambda}\frac{|\varepsilon_s''(z)|}{2\sqrt{\varepsilon_s'(z)}} \quad (2)$$

where $\alpha(z)$ and $T_s(z)$ are the soil attenuation coefficient (–) and soil temperature (K) at depth z, respectively, and ε_s' and ε_s'' are the real and imaginary part of the soil permittivity.

The single channel algorithm using the T_B^V measurements (SCA-V) adopted as the baseline retrieval algorithm of SMAP mission is utilized in this study to retrieve the θ_{liq}. The SCA-V is configured with above described microwave emission model in combination with the four-phase dielectric mixing model to retrieve the θ_{liq} using the ELBARA-III measured T_B^V as in Zheng et al. (2018c). The retrieved θ_{liq} is validated with the in-situ surface θ_{liq} taken from soil depths of 2.5 and 5 cm under both frozen and thawed soil conditions. The result of this assessment is presented in Section 3.4.

3. Results

3.1. Analyses of measurements

Fig. 2a shows the time series of ELBARA-III measured T_B^H and T_B^V at the incidence angles of 40° and 50° with a time interval of 30 min for the period between 7 August 2016 and 7 August 2018. The data gap noted for the ELBARA-III measurements is caused by a power supply failure. Fig. 2b and c show the time series of θ_{liq} and T_s measurements taken at soil depths of 2.5, 5, 25, 70 and 100 cm for the same time period. The data gap noted for the SMST measurements is related to a recording failure of the data loggers. In general, the soil is wet and unfrozen (Fig. 2b) with profile T_s measurements larger than 0 °C (Fig. 2c) in the warm season (e.g. May–October). During the warm season, the ELBARA-III measured T_B^H and T_B^V variations (Fig. 2a) generally follow the in-situ θ_{liq} dynamics, whereby both T_B^H and T_B^V decrease with increasing θ_{liq} (e.g., between August and October of 2016), and vice versa (e.g., between June and August of 2017). On the other hand, the surface soil starts freezing at the beginning of November (Fig. 2b) with the surface T_s measurements dropping below 0 °C (Fig. 2c). Following the soil freezing a sharp decrease in the measured θ_{liq} can be found (Fig. 2b), leading to the rapid increase in both T_B^H and T_B^V measured by the ELBARA-III radiometer (Fig. 2a). The frost depth reaches at the maximum (≈70 cm) in the mid of February, later on the surface soil starts thawing and the soil profile is totally thawed at the beginning of April. A rapid increase in the measured θ_{liq} can be found during the soil thawing period, resulting in a fast decrease in the

ELBARA-III T_B^P measurements. Two typical periods as highlighted in Fig. 2a are further selected for the following analyses: a cold period between 1 November 2017 and 17 March 2018 during which the surface soil layer is undergoing freezing and thawing, and a warm period from 7 August to 30 September 2016 where the soil is unfrozen, but subject to wetting and dry-down cycles.

Fig. 3a shows time series of ELBARA-III T_B^H and T_B^V measured at an incidence angle of 40° for the selected cold period along with the θ_{liq} measured at soil depths of 2.5, 5 and 10 cm. Fig. 3b displays time series of measured T_s at soil depths of 2.5, 5, 15 and 50 cm, and the T_{eff} calculated using Eqs. (1)–(2) with the profile SMST measurements (Section 2.1) as input. The T_{eff} is comparable to the T_s of 15 cm before the soil freezing when the near-surface θ_{liq} is relatively high, while it resembles better the dynamics of T_s at 50 cm when the soil is frozen that causes θ_{liq} to attain low values. It seems that the sampling depth of T_{eff} (δ_T) depends on the profile θ_{liq} values as also reported by Holmes et al. (2006) and Escorihuela et al. (2010), and the δ_T increases with the soil freezing, i.e. the decrease of θ_{liq}. The correlation between T_{eff} and T_s of different soil layers is given in Table 1, which shows that the T_{eff} is better correlated to T_s of deeper soil layers, and the best correlation is found between T_{eff} and T_s of 50 cm, i.e. δ_T is predicted as 50 cm for the selected cold period.

Diurnal cycles are clearly observed for both T_B^H and T_B^V in the cold period (Fig. 3a) due to the diurnal freezing and thawing of surface soil layer as shown in Zheng et al. (2017). Similar diurnal variations can be noted for the θ_{liq} measured at 2.5 cm soil depth, and the amplitude of the diurnal θ_{liq} cycles decreases with increasing soil depth. To further investigate the δ_{SM} of the L-band radiometer measurements, the correlation between the ELBARA-III measured T_B^P of different incidence angles and in-situ θ_{liq} taken from different soil depths is computed and given in Table 2. In contrast to the T_{eff}, both T_B^H and T_B^V of different incidence angles are better correlated to θ_{liq} of surface soil layer, and the δ_{SM} of the L-band radiometry is predicted as 2.5 cm for the cold period, which is in agreement with findings previously reported in Zheng et al. (2017), Roy et al. (2017), Rowlandson et al. (2018) and Williamson et al. (2018). It can be also found that the T_B^V measurements generally show better agreements with the in-situ θ_{liq} in comparison to the T_B^H measurements, which supports the selection of SCA-V as the SMAP baseline retrieval algorithm (Chan et al., 2016; Chan et al., 2018).

Fig. 3c shows the T_B^P measurements of 40° and θ_{liq} measurements of 2.5, 5 and 10 cm for the selected warm period, and the T_s measured at depths of 2.5, 5, 15 and 50 cm as well as the estimated T_{eff} are presented in Fig. 3d. The correlation between T_{eff} and T_s of different soil depths is also provided in Table 1. Highest correlation is found between T_{eff} and T_s of 15 cm for the selected warm period. In addition, the correlation between T_B^P of different incidence angles and θ_{liq} of different soil layers are given in Table 2. Highest correlation is found between T_B^V of different incidence angles and θ_{liq} of surface soil layer measured at 2.5 cm for the selected warm period, while the T_B^H measurements are better correlated with θ_{liq} measurements of slightly deeper soil layers, i.e. 5 and 10 cm for the incidence angle above and below the 60°, respectively. Since the T_B^H measurements are more sensitive to the surface roughness in comparison to the T_B^V measurements as indicated by Escorihuela et al. (2010), the δ_{SM} will be investigated in the following section through assessment of the sensitivity of land surface emission simulations to the soil depths at which the θ_{liq} measurements were taken.

Table 1
Coefficients of determination (R^2) computed between the T_{eff} and T_s at depths of 2.5, 5, 10, 15, 25, 50, 70 and 100 cm for the selected cold and warm periods.

Period	$T_{s,2.5}$	$T_{s,5}$	$T_{s,10}$	$T_{s,15}$	$T_{s,25}$	$T_{s,50}$	$T_{s,70}$	$T_{s,100}$
Cold-T_{eff}	0.33	0.55	0.69	0.82	0.92	**0.96**	0.94	0.91
Warm-T_{eff}	0.77	0.84	0.95	**0.97**	0.94	0.93	0.89	0.79

Boldface numbers are the highest R^2 values for both cold and warm periods.

3.2. Simulations of diurnal brightness temperature cycles

In order to investigate which soil depths for measuring θ_{liq} is most appropriate for reproducing the measured T_B^P, three numerical simulations are carried out for both selected cold and warm periods based on the τ-ω microwave emission model described in Section 2.2. Specifically, the measured θ_{liq} at soil depths of 2.5 (hereafter "Sim1"), 5 (Sim2) and 10 (Sim3) cm are respectively used to estimate the soil permittivity (ε_s) with the four-phase dielectric model. The T_{eff} is estimated with Eqs. (1)–(2), and the vegetation opacity and surface roughness parameterizations suggested by Zheng et al. (2018c) are also adopted.

Fig. 4a and b shows respectively the ELBARA-III T_B^H and T_B^V measurements and simulations produced by Sim1-Sim3 for a 40° incidence angle at a time interval of 30 min for the cold period. Table 3 lists the corresponding statistical errors, i.e. root mean-square error (RMSE), bias, unbiased RMSE (ubRMSE) and R^2, calculated between the measured and simulated T_B^P. From the figures we can deduce that all the numerical simulations tend to overestimate both T_B^H and T_B^V measurements during the soil freezing period between November and January, while T_B^H and T_B^V are better captured during the soil thawing period between February and March. The T_B^P simulations produced by the Sim1 using the θ_{liq} measurement of 2.5 cm show the best agreements with the ELBARA-III measurements as indicated by the highest R^2 values (0.86 for T_B^H and 0.90 for T_B^V) and lowest ubRMSE values (8.14 K for T_B^H and 5.14 K for T_B^V). The amplitudes of the measured diurnal T_B^P variations are also better reproduced by the Sim1, while Sim2 and Sim3 produced with θ_{liq} measurements from slightly deeper soil layers (i.e. 5 and 10 cm) are not able to match the amplitudes of the measured diurnal T_B^P cycles induced by the diurnal freezing and thawing of the surface soil layer. This demonstrates that the δ_{SM} of the L-band radiometry is close to 2.5 cm for the frozen soil in the cold period as was also reported by Zheng et al. (2017), Roy et al. (2017), Rowlandson et al. (2018) and Williamson et al. (2018).

Fig. 4c and d gives the T_B^P measurements and simulations for an incidence angle of 40° for the warm period, and the corresponding statistical errors are provided in Table 3. At the beginning of the selected warm period (7th to 22nd of August), the soil is subject to drying as a result of evapotranspiration as indicated by the strong θ_{liq} gradient between the surface soil layers (Fig. 3c), and the θ_{liq} at 2.5 cm dries faster than those measured at the slightly deeper soil layers (i.e. 5 and 10 cm). After the 25th of August, the soil is generally wet due to the rainfall, and this θ_{liq} gradient is relatively small. Both ELBARA-III measured T_B^H and T_B^V during the drying period (i.e. 7th to 22nd of August) are better captured with the simulations produced by Sim1 using the θ_{liq} from 2.5 cm, while both Sim2 and Sim3 using θ_{liq} measured respectively at 5 and 10 cm underestimate the magnitudes of measured T_B^P as well as the amplitudes of the diurnal cycles. For the wetting period after the 25th of August, the performances of all the numerical simulations are comparable to each other. Similar to the selected cold period, the simulations produced by the Sim1 provide the best agreements with the T_B^P measurements, indicating that the δ_{SM} of the L-band radiometry is also close to 2.5 cm for the thawed soil in the warm period. This is in agreement with both experimental and theoretical investigations reported previously (Wang, 1987; Escorihuela et al., 2010), which demonstrate that the δ_{SM} is about one-tenth of a λ, i.e., 2.1 cm for L-band radiometry.

3.3. Simulations of brightness temperature variations during satellite overpasses

As shown in Section 3.2, the δ_{SM} of the L-band radiometry is predicted to be close to 2.5 cm for both frozen and thawed soil conditions.

Table 2
R^2 calculated between the T_B^p measurements of different incidence angles and θ_{liq} measurements taken at depths of 2.5, 5, 10, 15, 25, 50, 70 and 100 cm for the selected cold and warm periods.

Period	T_B^p	$\theta_{liq,2.5}$	$\theta_{liq,5}$	$\theta_{liq,10}$	$\theta_{liq,15}$	$\theta_{liq,25}$	$\theta_{liq,50}$	$\theta_{liq,70}$	$\theta_{liq,100}$
Cold	V40	**0.91**	0.77	0.75	0.77	0.75	0.52	0.31	0.42
	V45	**0.92**	0.79	0.76	0.77	0.74	0.50	0.30	0.41
	V50	**0.93**	0.81	0.77	0.76	0.72	0.46	0.26	0.38
	V60	**0.92**	0.85	0.80	0.73	0.65	0.36	0.19	0.32
	V70	0.51	**0.63**	0.59	0.44	0.34	0.12	0.08	0.20
	H40	**0.85**	0.68	0.65	0.71	0.72	0.57	0.34	0.43
	H45	**0.85**	0.68	0.64	0.69	0.70	0.56	0.33	0.41
	H50	**0.85**	0.66	0.62	0.66	0.66	0.52	0.29	0.36
	H60	**0.83**	0.64	0.60	0.63	0.63	0.46	0.24	0.30
	H70	**0.81**	0.61	0.57	0.63	0.64	0.52	0.30	0.35
Warm	V40	**0.87**	0.82	0.86	0.81	0.67	0.68	0.24	0.04
	V45	**0.87**	0.82	0.85	0.80	0.67	0.68	0.23	0.03
	V50	**0.86**	0.81	0.85	0.78	0.69	0.65	0.206	0.03
	V60	**0.85**	0.79	0.82	0.75	0.68	0.62	0.19	0.02
	V70	**0.83**	0.75	0.79	0.72	0.63	0.62	0.20	0.03
	H40	0.85	0.84	**0.86**	0.83	0.68	0.69	0.24	0.03
	H45	0.82	0.83	**0.85**	0.81	0.68	0.66	0.22	0.02
	H50	0.78	0.81	**0.82**	0.78	0.70	0.61	0.18	0.01
	H60	0.69	**0.75**	0.75	0.71	0.69	0.52	0.12	0.00
	H70	0.65	**0.71**	0.70	0.67	0.64	0.50	0.12	0.00

Boldface numbers are the highest R^2 values for both cold and warm periods.

However, θ_{liq} measurements of the soil surface are generally taken from depth of 5 cm by the SMST monitoring networks that presently operational across the globe (Su et al., 2011; Colliander et al., 2017b), and these measurements were used to assess the performance of soil moisture products derived from the L-band SMAP and SMOS missions (Chan et al., 2016; Chen et al., 2017). To investigate the impact of the mismatch between the δ_{SM} and the shallowest depth at which θ_{liq} is measured by the above in-situ SMST networks on the T_B^p simulations, two numerical simulations are performed using the τ-ω microwave emission model for SMOS or SMAP descending/ascending overpasses, i.e. 6 am/pm of local time. Specifically, the θ_{liq} measurements taken from soil depths of 2.5 (hereafter "Sim1") and 5 (Sim2) cm are utilized to estimate the ε_s with the four-phase dielectric mixing model, respectively. Other settings are identical to the numerical simulations given in Section 3.2.

Fig. 5 shows time series of ELBARA-III T_B^p measurements and simulations (Sim1 and Sim2) for the incidence angle of 40° for both dawn (i.e. 6 am, Fig. 5a and b) and dusk overpasses (i.e. 6 pm, Fig. 5c and d) of SMOS and SMAP satellites from 7 August 2016 to 7 August 2018. Time series of θ_{liq} measured at 2.5 and 5 cm for the same time period taken at 6 am and 6 pm are also presented in Fig. 5a and c, respectively. The statistical errors calculated between the ELBARA-III T_B^p measurements and the simulations produced by Sim1 and Sim2 are given in Table 4. In general, the dynamics of θ_{liq} measurements taken from soil depths of 2.5 and 5 cm are comparable to each other, and the correlation coefficients are 0.90 and 0.82 for dawn and dusk overpasses, respectively. In comparison to the Sim2 using the θ_{liq} of 5 cm, the T_B^p simulations produced by the Sim1 using the θ_{liq} of 2.5 cm capture better the dynamics of ELBARA-III measurements with higher R^2 values, i.e. 0.54 vs. 0.37 and 0.65 vs. 0.41 on average for the T_B^H and T_B^V, respectively. The Sim1 simulations result in a lower ubRMSE, on average 14% (3.16 K) and 22% (3.36 K) for the T_B^H and T_B^V respectively, in comparison to the Sim2 simulations.

3.4. Retrieval of soil liquid water content

Fig. 6a shows time series of θ_{liq} measured at soil depths of 2.5 and 5 cm and the SCA-V retrievals from the ELBARA-III measured T_B^V at the incidence angle of 40° for the cold period. Table 5 lists the statistical errors computed between the θ_{liq} measurements of 2.5 and 5 cm and the

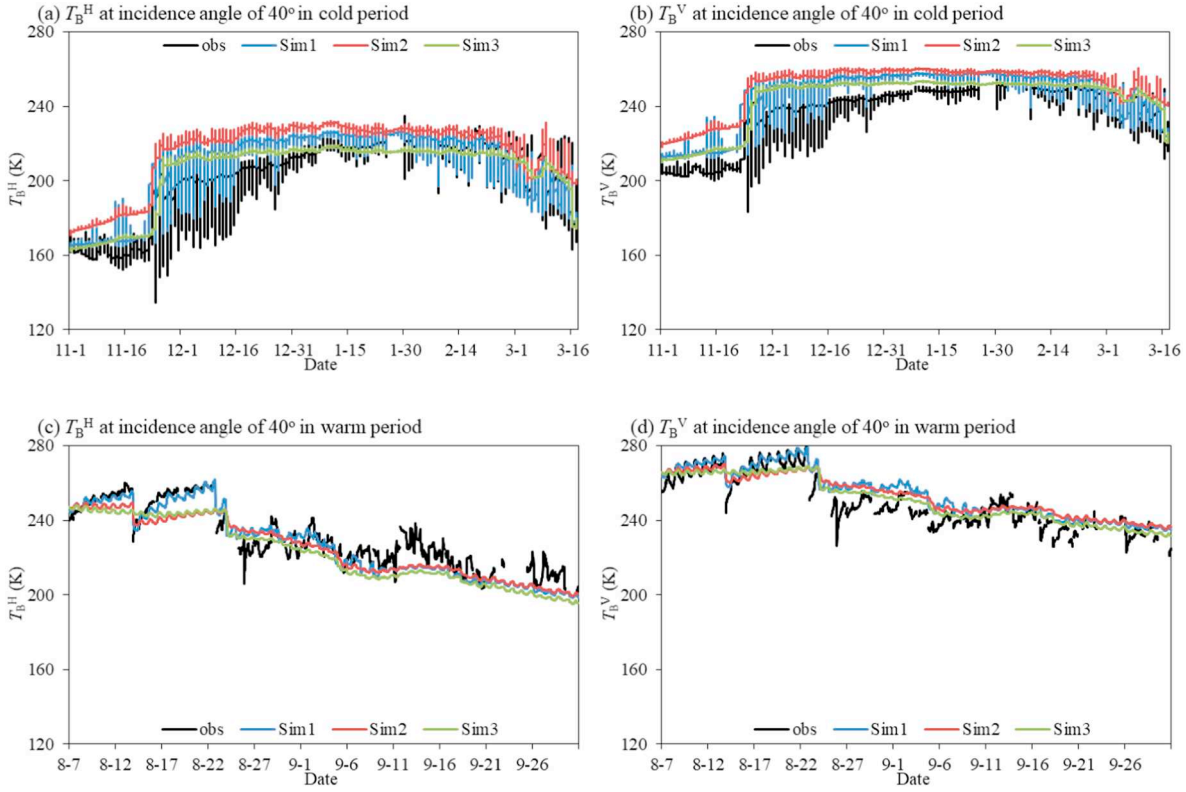

Fig. 4. Time series of simulated and measured (a, c) T_B^H and (b, d) T_B^V at incidence angle of 40° for the selected cold (2017.11.1–2018.3.17) and warm (2016.8.7–2016.9.30) periods.

Table 3
Statistical errors calculated between the T_B^p measurements and simulations at incidence angle of 40° for the selected cold and warm periods.

Simulations	T_B^H				T_B^V			
	ubRMSE (K)	Bias (K)	RMSE (K)	R^2	ubRMSE (K)	Bias (K)	RMSE (K)	R^2
Cold Period								
Sim1 (2.5 cm)	8.14	7.45	11.04	0.86	5.14	9.58	10.87	0.90
Sim2 (5 cm)	12.19	16.63	20.62	0.68	8.28	15.86	17.89	0.75
Sim3 (10 cm)	12.79	5.50	13.92	0.65	8.44	8.54	12.01	0.72
Warm Period								
Sim1 (2.5 cm)	7.12	-2.63	7.59	0.85	4.94	5.45	7.35	0.87
Sim2 (5 cm)	7.55	-4.76	8.93	0.78	6.43	3.92	7.53	0.80
Sim3 (10 cm)	7.45	-7.05	10.26	0.80	5.76	1.80	6.04	0.83

SCA-V retrievals. From the figure we can find that the SCA-V retrievals overestimate the θ_{liq} measurements during the soil freezing period between November and January due to the overestimation of T_B^V earlier noted for the emission modelling (Fig. 4a). The SCA-V retrievals capture well the dynamics of θ_{liq} measurements during the soil thawing period between February and March. Notably, the SCA-V retrievals match better with the θ_{liq} measurements of 2.5 cm, which results in an ubRMSE and bias about 36% (i.e. 0.017 $m^3 m^{-3}$) and 55% (i.e. 0.03 $m^3 m^{-3}$) lower in comparison to the statistical errors calculated as the SCA-V retrievals versus the θ_{liq} measurements of 5 cm. This confirms the previous finding that the δ_{SM} of the L-band radiometry is closer to 2.5 cm than 5 cm for the frozen soil condition (Section 3.2).

Fig. 6b shows the measured and retrieved θ_{liq} for the warm period, and the corresponding statistical errors are provided in Table 5. Similar to the cold period, the SCA-V retrievals are best matched by the θ_{liq} measurements of 2.5 cm, especially during the dry-down period from 7th to 22nd of August. The validation statistics computed with the θ_{liq} measurements of 2.5 cm are also better in compared to the statistics

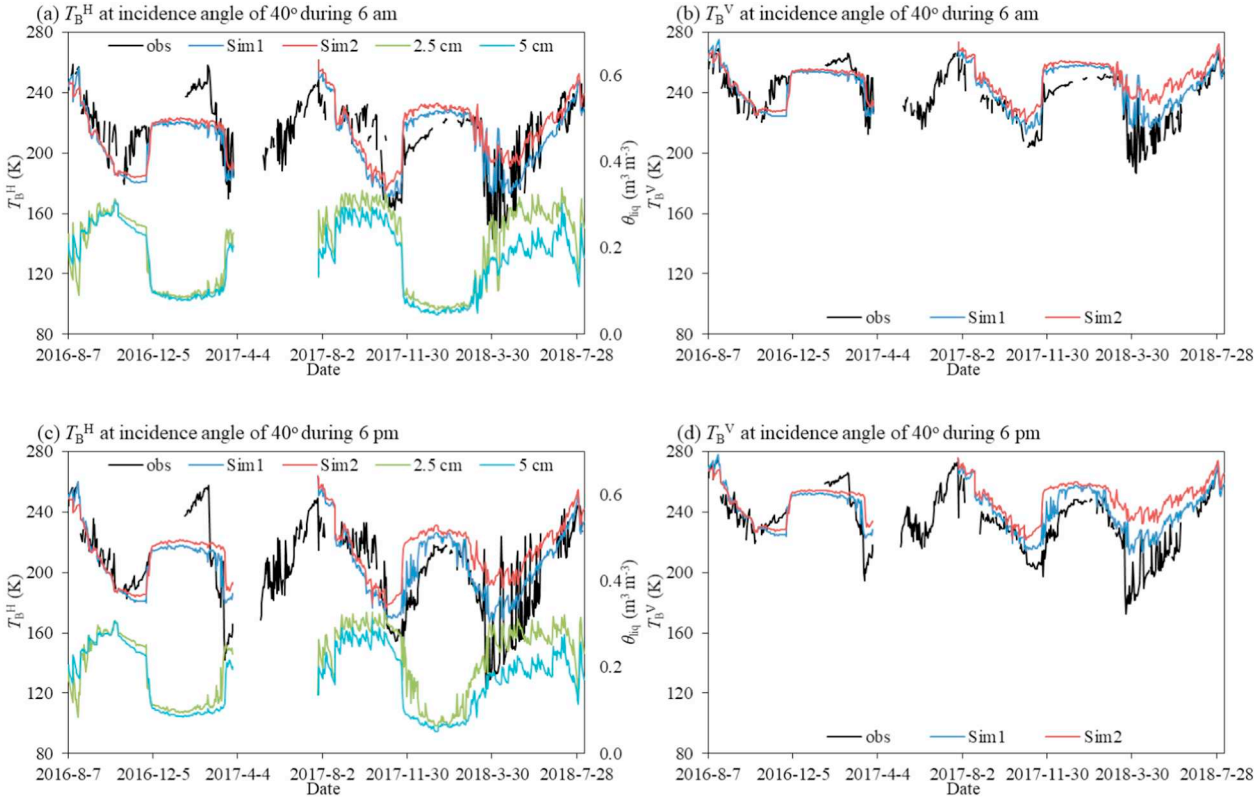

Fig. 5. Time series of simulated and measured (a, c) T_B^H and (b, d) T_B^V at incidence angle of 40° during 6 am and 6 pm of local time from 7 August 2016 to 7 August 2018. The measured θ_{liq} at soil depths of 2.5 and 5 cm are also shown in (a) and (c).

Table 4
Statistical errors calculated between the T_B^P measurements and simulations at incidence angle of 40° during 6 am and 6 pm of local time from 7 August 2016 to 7 August 2018.

Simulations	T_B^H				T_B^V			
	ubRMSE (K)	Bias (K)	RMSE (K)	R^2	ubRMSE (K)	Bias (K)	RMSE (K)	R^2
6 am								
Sim1 (2.5 cm)	17.94	-5.19	18.68	0.50	11.51	4.35	12.30	0.60
Sim2 (5 cm)	19.66	0.55	19.67	0.38	13.82	9.07	16.53	0.42
6 pm								
Sim1 (2.5 cm)	20.07	2.60	20.23	0.58	11.77	7.76	14.09	0.70
Sim2 (5 cm)	24.67	11.18	27.08	0.36	16.18	14.57	21.77	0.41

calculated with the θ_{liq} measurements of 5 cm, which supports that the δ_{SM} is also close to 2.5 cm for the thawed soil condition.

4. Conclusion

This study investigates the sampling depth (δ_{SM}) of the L-band radiometry for monitoring surface soil moisture and freeze-thaw dynamics, as well as to assess the impact of the mismatch between the δ_{SM} and measurement depth of θ_{liq} on the T_B^P simulations and the validation of θ_{liq} retrievals. Two years of T_B^P measurements at a time interval of 30 min are collected by the ESA funded ELBARA-III radiometer deployed in a Tibetan meadow ecosystem. Besides, a vertically dense profile SMST measurement is performed next to the radiometer.

A correlation analysis between the estimated T_{eff} and T_s measurements taken from different soil depths shows that the sampling depth of the T_{eff} (δ_T) depends on the soil moisture conditions, and the δ_T is predicted to be about 50 and 15 cm for the cold dry and wet warm period, respectively. On the other hand, both the correlation analysis and numerical simulations of T_B^P using θ_{liq} measurements taken from different surface soil layers demonstrate that the δ_{SM} is predicted to be closest to 2.5 cm regardless of the season and freeze-thaw state. This is in agreement with previously reported experimental and theoretical investigations (Wang, 1987; Escorihuela et al., 2010; Zheng et al., 2017; Rowlandson et al., 2018) that the δ_{SM} is about one-tenth of a λ, i.e., 2.1 cm for the L-band radiometry. The reason for the low δ_{SM} value noted for the frozen soil is due to the fact that the changing permittivity

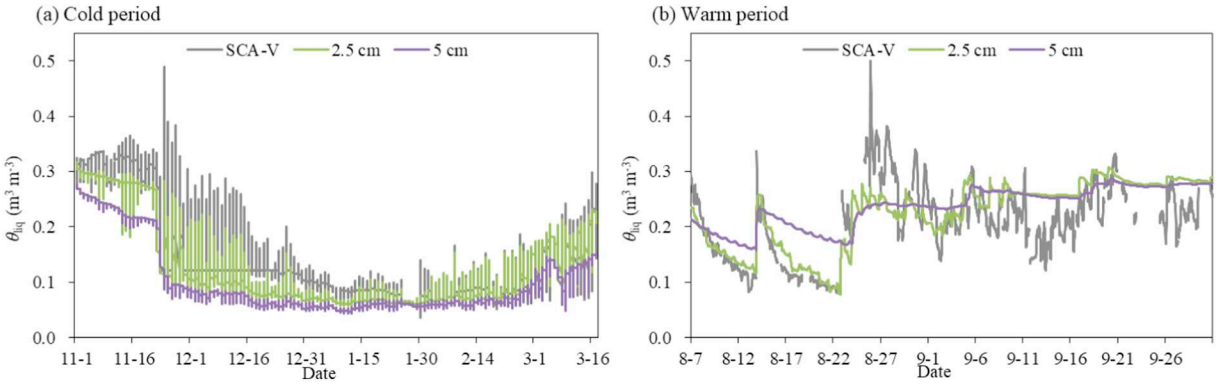

Fig. 6. Time series of θ_{liq} measured at soil depths of 2.5 and 5 cm and the retrievals obtained by the SCA-V approach for the selected (a) cold (2017.11.1–2018.3.17), and (b) warm (2016.8.7–2016.9.30) periods.

Table 5
Statistical errors calculated between the θ_{liq} measured at soil depths of 2.5 and 5 cm and the SCA-V retrievals for the selected cold and warm periods.

Measurements	Cold period				Warm period			
	ubRMSE ($m^3 m^{-3}$)	Bias ($m^3 m^{-3}$)	RMSE ($m^3 m^{-3}$)	R^2	ubRMSE ($m^3 m^{-3}$)	Bias ($m^3 m^{-3}$)	RMSE ($m^3 m^{-3}$)	R^2
2.5 cm	0.030	0.025	0.039	0.88	0.051	−0.013	0.053	0.48
5 cm	0.047	0.055	0.072	0.73	0.055	−0.027	0.061	0.37

of surface soil layer caused by the diurnal freeze–thaw transition dominates the T_B^P variations as reported in Zheng et al. (2017).

Although the δ_{SM} is predicted to be 2.5 cm for the L-band microwave radiometry, the surface θ_{liq} measurements are generally taken at a depth of 5 cm by current in-situ SMST networks operated on the Tibetan Plateau, and these measurements were utilized to assess the performance of soil moisture retrievals from L-band satellite missions (Dente et al., 2012; Chen et al., 2017). Numerical simulations of T_B^P using θ_{liq} measurements taken from soil depths of 2.5 and 5 cm indicate that the simulations using the θ_{liq} measurements of 2.5 cm produce an ubRMSE about 14% (3.16 K, for T_B^H) and 22% (3.36 K, for T_B^V) on average lower in comparison to the simulations using the θ_{liq} measurements of 5 cm. Furthermore, the comparison between the θ_{liq} retrievals based on the SCA-V from the ELBARA-III measured T_B^V and the in-situ θ_{liq} shows that the SCA-V retrievals are closest to the θ_{liq} measurements of 2.5 cm for both cold and warm periods. This confirms that the δ_{SM} is close to 2.5 cm for the L-band microwave radiometry measurements of frozen and thawed soil conditions.

Therefore, the in-situ SMST monitoring networks are recommended to measure the θ_{liq} at shallower soil depth close to the surface (i.e. 2.5 cm) for better reproducing the L-band radiometry measurements. An alternative way is to use the mechanistic soil model to predict the θ_{liq} of surface soil layer as shown in Escorihuela et al. (2010) and Zheng et al. (2017). These findings are crucial for developing soil moisture calibration/validation strategies as part of satellite missions relying on the L-band radiometry. For example, Fernandez-Moran et al. (2017) recently showed that an alternative SMOS soil moisture product (i.e. SMOS-IC) tends to be drier than the ECMWF dataset due to the mismatch between the sampling depths of two products. A better understanding of the sampling depth can also assist in appreciating the application-value of satellite based soil moisture products.

Acknowledgments

This study was supported by funding from the National Natural Science Foundation of China (Grant No. 41871273, 41530529 and 41630856) and the Netherlands Organisation for Scientific Research (Project No. ALW-GO/14-29). The authors are grateful to ESA for offering the ELBARA-III radiometer. Donghai Zheng is supported by the Chinese Academy of Sciences granted Hundred Talent Program.

References

Chan, S.K., Bindlish, R., O'Neill, P.E., Njoku, E., Jackson, T., Colliander, A., Chen, F., Burgin, M., Dunbar, S., Piepmeier, J., 2016. Assessment of the SMAP passive soil moisture product. IEEE Trans. Geosci. Remote Sens. 54, 4994–5007.

Chan, S.K., Bindlish, R., O'Neill, P., Jackson, T., Njoku, E., Dunbar, S., Chaubell, J., Piepmeier, J., Yueh, S., Entekhabi, D., Colliander, A., Chen, F., Cosh, M.H., Caldwell, T., Walker, J., Berg, A., McNairn, H., Thibeault, M., Martínez-Fernández, J., Uldall, F., Seyfried, M., Bosch, D., Starks, P., Holifield Collins, C., Prueger, J., van der Velde, R., Asanuma, J., Palecki, M., Small, E.E., Zreda, M., Calvet, J., Crow, W.T., Kerr, Y., 2018. Development and assessment of the SMAP enhanced passive soil moisture product. Remote Sens. Environ. 204, 931–941.

Chen, Y., Yang, K., Qin, J., Cui, Q., Lu, H., La, Z., Han, M., Tang, W., 2017. Evaluation of SMAP, SMOS, and AMSR2 soil moisture retrievals against observations from two networks on the Tibetan Plateau. Journal of Geophysical Research: Atmospheres 122, 2016JD026388.

Choudhury, B., Schmugge, T., Mo, T., 1982. A parameterization of effective soil temperature for microwave emission. Journal of Geophysical Research: Oceans 87, 1301–1304.

Colliander, A., Cosh, M.H., Misra, S., Jackson, T.J., Crow, W.T., Chan, S., Bindlish, R., Chae, C., Holifield Collins, C., Yueh, S.H., 2017a. Validation and scaling of soil moisture in a semi-arid environment: SMAP validation experiment 2015 (SMAPVEX15). Remote Sens. Environ. 196, 101–112.

Colliander, A., Jackson, T., Bindlish, R., Chan, S., Das, N., Kim, S., Cosh, M., Dunbar, R., Dang, L., Pashaian, L., 2017b. Validation of SMAP surface soil moisture products with core validation sites. Remote Sens. Environ. 191, 215–231.

Dente, L., Su, Z., Wen, J., 2012. Validation of SMOS soil moisture products over the Maqu and Twente regions. Sensors 12, 9965–9986.

Derksen, C., Xu, X., Dunbar, R.S., Colliander, A., Kim, Y., Kimball, J.S., Black, T.A., Euskirchen, E., Langlois, A., Loranty, M.M., 2017. Retrieving landscape freeze/thaw state from Soil Moisture Active Passive (SMAP) radar and radiometer measurements. Remote Sens. Environ. 194, 48–62.

Entekhabi, D., Njoku, E.G., Neill, P.E.O., Kellogg, K.H., Crow, W.T., Edelstein, W.N., Entin, J.K., Goodman, S.D., Jackson, T.J., Johnson, J., Kimball, J., Piepmeier, J.R., Koster, R.D., Martin, N., McDonald, K.C., Moghaddam, M., Moran, S., Reichle, R., Shi, J.C., Spencer, M.W., Thurman, S.W., Tsang, L., Zyl, J.V., 2010. The Soil Moisture Active Passive (SMAP) Mission. Proc. IEEE 98, 704–716.

Escorihuela, M.-J., Chanzy, A., Wigneron, J.-P., Kerr, Y., 2010. Effective soil moisture sampling depth of L-band radiometry: a case study. Remote Sens. Environ. 114, 995–1001.

Fernandez-Moran, R., Al-Yaari, A., Mialon, A., Mahmoodi, A., Al Bitar, A., De Lannoy, G., Rodriguez-Fernandez, N., Lopez-Baeza, E., Kerr, Y., Wigneron, J.-P., 2017. SMOS-IC: an alternative SMOS soil moisture and vegetation optical depth product. 9, 457.

Holmes, T., De Rosnay, P., De Jeu, R., Wigneron, R.P., Kerr, Y., Calvet, J.C., Escorihuela, M., Saleh, K., Lemaître, F., 2006. A new parameterization of the effective temperature

for L band radiometry. Geophys. Res. Lett. 33.
Jin, R., Li, X., Che, T., 2009. A decision tree algorithm for surface soil freeze/thaw classification over China using SSM/I brightness temperature. Remote Sens. Environ. 113, 2651–2660.
Kerr, Y.H., Waldteufel, P., Wigneron, J.-P., Martinuzzi, J., Font, J., Berger, M., 2001. Soil moisture retrieval from space: the Soil Moisture and Ocean Salinity (SMOS) mission. IEEE Trans. Geosci. Remote Sens. 39, 1729–1735.
Kerr, Y.H., Waldteufel, P., Richaume, P., Wigneron, J.P., Ferrazzoli, P., Mahmoodi, A., Al Bitar, A., Cabot, F., Gruhier, C., Juglea, S.E., 2012. The SMOS soil moisture retrieval algorithm. IEEE Trans. Geosci. Remote Sens. 50, 1384–1403.
Koster, R.D., Dirmeyer, P.A., Guo, Z., Bonan, G., Chan, E., Cox, P., Gordon, C.T., Kanae, S., Kowalczyk, E., Lawrence, D., Liu, P., Lu, C.-H., Malyshev, S., McAvaney, B., Mitchell, K., Mocko, D., Oki, T., Oleson, K., Pitman, A., Sud, Y.C., Taylor, C.M., Verseghy, D., Vasic, R., Xue, Y., Yamada, T., 2004. Regions of strong coupling between soil moisture and precipitation. Science 305, 1138–1140.
Li, X., Jin, R., Pan, X., Zhang, T., Guo, J.J., 2012. Changes in the near-surface soil freeze–thaw cycle on the Qinghai-Tibetan Plateau. International Journal of Applied Earth Observation and Geoinformation 17, 33–42.
Li, C., Lu, H., Yang, K., Han, M., Wright, J., Chen, Y., Yu, L., Xu, S., Huang, X., Gong, W., 2018. The evaluation of SMAP enhanced soil moisture products using high-resolution model simulations and in-situ observations on the Tibetan Plateau. Remote Sens. 10, 535.
Lv, S., Zeng, Y., Wen, J., Zhao, H., Su, Z., 2018. Estimation of penetration depth from soil effective temperature in microwave radiometry. Remote Sens. 10, 519.
Mcnairn, H., Jackson, T.J., Wiseman, G., Bélair, S., Berg, A., Bullock, P., Colliander, A., Cosh, M.H., Kim, S.B., Magagi, R., 2015. The Soil Moisture Active Passive Validation Experiment 2012 (SMAPVEX12): prelaunch calibration and validation of the SMAP soil moisture algorithms. IEEE Transactions on Geoscience & Remote Sensing 53, 2784–2801.
Mo, T., Choudhury, B., Schmugge, T., Wang, J., Jackson, T., 1982. A model for microwave emission from vegetation-covered fields. Journal of Geophysical Research: Oceans 87, 11229–11237.
Montzka, C., Bogena, H.R., Weihermuller, L., Jonard, F., Bouzinac, C., Kainulainen, J., Balling, J.E., Loew, A., Dall'Amico, J.T., Rouhe, E., 2013. Brightness temperature and soil moisture validation at different scales during the SMOS validation campaign in the Rur and Erft catchments, Germany. IEEE Transactions on Geoscience & Remote Sensing 51, 1728–1743.
Naderpour, R., Schwank, M., Mätzler, C., 2017. Davos-Laret Remote Sensing Field Laboratory: 2016/2017 Winter Season L-band Measurements Data-processing and Analysis. vol. 9. pp. 1185.
O'Neill, P., Njoku, E., Jackson, T., Chan, S., Bindlish, R., 2015. SMAP Algorithm Theoretical Basis Document: Level 2 & 3 Soil Moisture (Passive) Data Products. In: Jet Propulsion Lab., California Inst. Technol., Pasadena, CA, USA, JPL D-66480.
Panciera, R., Walker, J.P., Jackson, T.J., Gray, D.A., Tanase, M.A., Ryu, D., Monerris, A., Yardley, H., Rudiger, C., Wu, X., 2013. The Soil Moisture Active Passive Experiments (SMAPEx): toward soil moisture retrieval from the SMAP mission. IEEE Transactions on Geoscience & Remote Sensing 52, 490–507.
Pellarin, T., Mialon, A., Biron, R., Coulaud, C., Gibon, F., Kerr, Y., Lafaysse, M., Mercier, B., Morin, S., Redor, I., 2016. Three years of L-band brightness temperature measurements in a mountainous area: topography, vegetation and snowmelt issues. Remote Sens. Environ. 180, 85–98.
Raju, S., Chanzy, A., Wigneron, J.-P., Calvet, J.-C., Kerr, Y., Laguerre, L., 1995. Soil moisture and temperature profile effects on microwave emission at low frequencies. Remote Sens. Environ. 54, 85–97.
Rautiainen, K., Lemmetyinen, J., Pulliainen, J., Vehvilainen, J., Drusch, M., Kontu, A., Kainulainen, J., Seppanen, J., 2012. L-band radiometer observations of soil processes in boreal and subarctic environments. IEEE Trans. Geosci. Remote Sens. 50, 1483–1497.
Rautiainen, K., Lemmetyinen, J., Schwank, M., Kontu, A., Ménard, C.B., Maetzler, C., Drusch, M., Wiesmann, A., Ikonen, J., Pulliainen, J., 2014. Detection of soil freezing from L-band passive microwave observations. Remote Sens. Environ. 147, 206–218.
Rautiainen, K., Parkkinen, T., Lemmetyinen, J., Schwank, M., Wiesmann, A., Ikonen, J., Derksen, C., Davydov, S., Davydova, A., Boike, J., Langer, M., Drusch, M., Pulliainen, J., 2016. SMOS prototype algorithm for detecting autumn soil freezing. Remote Sens. Environ. 180, 346–360.
Rowlandson, T.L., Berg, A.A., Roy, A., Kim, E., Pardo Lara, R., Powers, J., Lewis, K., Houser, P., Mcdonald, K., Toose, P., 2018. Capturing agricultural soil freeze/thaw state through remote sensing and ground observations: a soil freeze/thaw validation campaign. Remote Sens. Environ. 211, 59–70.
Roy, A., Toose, P., Williamson, M., Rowlandson, T., Derksen, C., Royer, A., Berg, A.A., Lemmetyinen, J., Arnold, L., 2017. Response of L-band brightness temperatures to freeze/thaw and snow dynamics in a prairie environment from ground-based radiometer measurements. Remote Sens. Environ. 191, 67–80.
Schwank, M., Stahli, M., Wydler, H., Leuenberger, J., Matzler, C., Fluhler, H., 2004. Microwave L-band emission of freezing soil. IEEE Trans. Geosci. Remote Sens. 42, 1252–1261.
Schwank, M., Wiesmann, A., Werner, C., Mätzler, C., Weber, D., Murk, A., Völksch, I., Wegmüller, U., 2010. ELBARA II, an L-band radiometer system for soil moisture research. Sensors 10, 584–612.
Schwank, M., Wigneron, J.P., Lopez-Baeza, E., Volksch, I., Matzler, C., Kerr, Y.H., 2012. L-band radiative properties of vine vegetation at the MELBEX III SMOS cal/val site. IEEE Transactions on Geoscience & Remote Sensing 50, 1587–1601.
Schwank, M., Naderpour, R., Mätzler, C., 2018. "Tau-omega"- and two-stream emission models used for passive L-band retrievals: application to close-range measurements over a forest. Remote Sens. 10, 1868.
Su, Z., Wen, J., Dente, L., van der Velde, R., Wang, L., Ma, Y., Yang, K., Hu, Z., 2011. The Tibetan Plateau observatory of plateau scale soil moisture and soil temperature (Tibet-Obs) for quantifying uncertainties in coarse resolution satellite and model products. Hydrol. Earth Syst. Sci. 15, 2303–2316.
Wang, J.R., 1987. Microwave emission from smooth bare fields and soil moisture sampling depth. IEEE Transactions on Geoscience & Remote Sensing GE-25, 616–622.
Wigneron, J.P., Jackson, T.J., O'Neill, P., De Lannoy, G., de Rosnay, P., Walker, J.P., Ferrazzoli, P., Mironov, V., Bircher, S., Grant, J.P., Kurum, M., Schwank, M., Munoz-Sabater, J., Das, N., Royer, A., Al-Yaari, A., Al Bitar, A., Fernandez-Moran, R., Lawrence, H., Mialon, A., Parrens, M., Richaume, P., Delwart, S., Kerr, Y., 2017. Modelling the passive microwave signature from land surfaces: a review of recent results and application to the L-band SMOS & SMAP soil moisture retrieval algorithms. Remote Sens. Environ. 192, 238–262.
Wilheit, T.T., 1978. Radiative transfer in a plane stratified dielectric. IEEE Trans. Geosci. Electron. 16, 138–143.
Williamson, M., Rowlandson, T.L., Berg, A.A., Roy, A., Toose, P., Derksen, C., Arnold, L., Tetlock, E., 2018. L-band radiometry freeze/thaw validation using air temperature and ground measurements. Remote Sensing Letters 9, 403–410.
Yang, K., Qin, J., Zhao, L., Chen, Y., Tang, W., Han, M., Lazhu, Chen, Z., Lv, N., Ding, B., Wu, H., & Lin, C. (2013). A multiscale soil moisture and freeze–thaw monitoring network on the third pole. Bull. Am. Meteorol. Soc., 94, 1907–1916.
Zheng, D., Wang, X., van der Velde, R., Zeng, Y., Wen, J., Wang, Z., Schwank, M., Ferrazzoli, P., Su, Z., 2017. L-band microwave emission of soil freeze-thaw process in the third pole environment. IEEE Trans. Geosci. Remote Sens. 55, 5324–5338.
Zheng, D., van der Velde, R., Su, Z., Wen, J., Wang, X., Yang, K., 2018a. Impact of soil freeze-thaw mechanism on the runoff dynamics of two Tibetan rivers. J. Hydrol. 563, 382–394.
Zheng, D., Velde, R.v.d., Wen, J., Wang, X., Ferrazzoli, P., Schwank, M., Colliander, A., Bindlish, R., Su, Z., 2018b. Assessment of the SMAP soil emission model and soil moisture retrieval algorithms for a Tibetan desert ecosystem. IEEE Trans. Geosci. Remote Sens. 56, 3786–3799.
Zheng, D., Wang, X., van der Velde, R., Ferrazzoli, P., Wen, J., Wang, Z., Schwank, M., Colliander, A., Bindlish, R., Su, Z., 2018c. Impact of surface roughness, vegetation opacity and soil permittivity on L-band microwave emission and soil moisture retrieval in the third pole environment. Remote Sens. Environ. 209, 633–647.